ADVANCED PHOTONICS RESEARCH Open Access
www.adpr-journal.com

Building Paraxial Optical Skyrmions Using Rational Maps

*Claire Cisowski, Calum Ross, and Sonja Franke-Arnold**

A simple mathematical expression based on rational maps to describe all optical paraxial skyrmion known to date, including Néel-type and Bloch-type skyrmions, bimerons, and anti-skyrmions, is introduced. This expression is derived solely from topological considerations and outlines the rules that fully polarized paraxial light fields must obey to qualify as optical skyrmions. It is shown that rational maps can be implemented experimentally by superposing a pair of orthogonally polarized Laguerre–Gaussian modes. Novel optical skyrmion fields, called multi-skyrmions, are obtained upon generalizing the proposed expression, laying the foundation for the exploration of skyrmion nucleation and annihilation mechanisms in optics.

1. Introduction

Skyrmions were introduced as minimal energy field configurations in a nonlinear scalar field model of the atomic nucleus by Tony Skyrme in 1962.[1] Skyrme's model is founded on an elegant topological construction,[2] which confers a universal dimension to skyrmions. Consequently, skyrmions, as topological objects, have been identified in various areas of physics including condensed matter physics,[3] string theory,[4] magnetism,[5] in sound waves,[6] and recently in optics.

Research on optical skyrmions is still in its infancy. First witnessed in the evanescent field of surface plasmon polaritons in 2018,[7,8] they have since been generated in freely propagating light fields in the paraxial[9–11] and the nonparaxial[12] regimes, and the first nonlocal quantum skyrmions have already been observed.[13] Combining phase information with the polarization profile of paraxial skyrmions has uncovered novel optical topological structures called Hopfions.[14,15] Initially, research efforts were focused on modeling paraxial optical skyrmions on their magnetic counterparts,[16] and an analogy justified because both represent "baby" skyrmions: skyrmion fields defined in a 2D space.[17,18] In the following, we will refer to such 2D skyrmions as skyrmions for simplicity. Optical polarization textures that have been investigated include Néel-type and Bloch-type skyrmions,[9,12] bimerons, and anti-skyrmions.[10,19] These fields can be generated on-demand with digital micromirror devices,[11] a technology that enables the dynamic generation of reconfigurable polarization structures. Optical skyrmions are set to become versatile light sources for the controlled excitation of skyrmion fields in matter,[20,21] and thus they could play a central role in the development of future data storage devices.[22,23]

While the spin texture of magnetic skyrmions is defined by the crystal structure, conservation laws, and energy minimization, such constraints seem to be missing in optics. In principle, one may generate arbitrary polarization textures, limited only by Maxwell's equations. Here we set out to provide a unifying framework capable of describing all optical skyrmions based entirely on topological considerations. This article introduces an analytical expression to construct general paraxial optical skyrmion fields based on rational maps, a method that has never been explicitly employed to construct optical skyrmions. Rational maps entered the world of skyrmions in 1998.[24] In Skyrme's original model, a skyrmion is a field solution of the equation that minimizes the energy functional of the system. As Skyrme's field equation is not integrable, one must often resort to numerical techniques to compute the minimum energy configurations, which can, however, be time consuming and requires significant computational resources. To facilitate this task, Houghton et al. proposed the use of rational maps to find approximate solutions.[24] This method turned out to be rather accurate, especially for skyrmions of low skyrmion number.[25] Rational maps had previously been employed to construct Bogomolny–Prasad–Sommerfield (BPS) monopoles.[26] It was the realization that BPS monopoles and low energy skyrmions possess similar energy densities, symmetries, and spatial distributions that led Houghton et al. to propose rational maps in the context of skyrmions. While Skyrme's field equation describes skyrmions in three dimensions, rational maps are equally capable of describing 2D skyrmion fields,[27,28] allowing us to use them for the

C. Cisowski
School of Physics and Astronomy
University of Glasgow
Glasgow G12 8QQ, UK

C. Ross
Department of Mathematics
University College London
London WC1E 6BT, UK

C. Ross
Department of Physics and Research and Education Center for Natural Sciences
Keio University
Hiyoshi 4-1-1, Yokohama, Kanagawa 223-8521, Japan

S. Franke-Arnold
School of Physics and Astronomy
University of Glasgow
Glasgow G12 8QQ, UK
E-mail: sonja.franke-arnold@glasgow.ac.uk

The ORCID identification number(s) for the author(s) of this article can be found under https://doi.org/10.1002/adpr.202200350.

DOI: 10.1002/adpr.202200350

construction of optical skyrmions. There are several advantages to using rational maps for the construction of optical skyrmions. First, as rational maps are direct applications of the topological skyrmion model, they allow us to distinguish topological features from beam characteristics that are merely due to their experimental realization. Second, they provide guidelines for generating novel optical skyrmion fields, as we will demonstrate in the second part of this paper with the example of optical multi-skyrmion fields. Finally, rational maps lay the foundation for exploring the difference between optical skyrmion fields and their magnetic counterparts. Indeed, expressing optical skyrmions in terms of rational maps effectively uncovers the equations that define optical skyrmions, marking the beginning of investigations of their physical interpretation.

2. Topology of 2D Skyrmions

Optical skyrmions are characterized by specific polarization textures. Each position (x, y) in a plane Γ transverse to the propagation direction of a light beam can be uniquely mapped to a reduced Stokes vector $\mathbf{S}(x, y) = [\mathbf{S}_1(x, y), \mathbf{S}_2(x, y), \mathbf{S}_3(x, y)]^T$.[9] The tip of the unit vector $\mathbf{S}(x, y)$ defines a point on the Poincaré sphere representing the local polarization state, which corresponds to a polarization ellipse. We refer to the mapping from the plane (the beam profile) to the sphere (the Poincaré sphere) as a paraxial optical skyrmion field. An equivalent definition holds for all 2D skyrmion fields, including magnetic skyrmions.[18,29]

In the following, we will show that an integer skyrmion number N can be associated with this mapping if the plane of the beam profile Γ can be mapped to a unit sphere Σ. This causes the skyrmion field to become a map between two spheres, Σ and the Poincaré sphere, as illustrated in **Figure 1**. This process is usually accomplished using an inverse stereographic projection.

An inverse stereographic projection identifies spatial infinity on the plane Γ with a single point on the unit-sphere Σ and then uses this point as a projection point to image all remaining spatial positions (x, y) on Γ onto points on Σ. Let us consider, for example, the case where the projection point is the North Pole of Σ, with the coordinates $\mathbf{r} = (\mathbf{r}_1, \mathbf{r}_2, \mathbf{r}_3) = (0, 0, 1)$, and Γ is the plane passing through the equator of the unit sphere, centered around the center of the beam profile. A straight line from the North Pole to the plane passes uniquely through one point on the sphere, mapping a point (x, y) in Γ to the point

$$\mathbf{r} = (2x, 2y, x^2 + y^2 - 1)/(1 + x^2 + y^2) \tag{1}$$

on Σ. The vector $\mathbf{S}(x, y)$, attached to a point (x, y) in Γ, now becomes attached to the image of that point, $\mathbf{r}$, in Σ. We note that the inverse stereographic projection requires a uniform polarization state $\mathbf{S}(x, y)$ in all directions at spatial infinity. This situation occurs naturally in Skyrme's model as it ensures that the energy gradient is divergence-less, and hence that the field energy is finite.[30] In paraxial optical skyrmion beams, this condition needs to be imposed in the design of the light field and typically will be met at a finite radius rather than at infinity, within the measurable beam intensity profile, due to the radial profile of the constituting optical modes. The overall polarization texture $\mathbf{S}(\mathbf{r})$, hence $\mathbf{S}(x, y)$ is now characterized by the mapping between Σ and the Poincaré sphere, which varies from skyrmion field to skyrmion field. We shall provide the rules for these

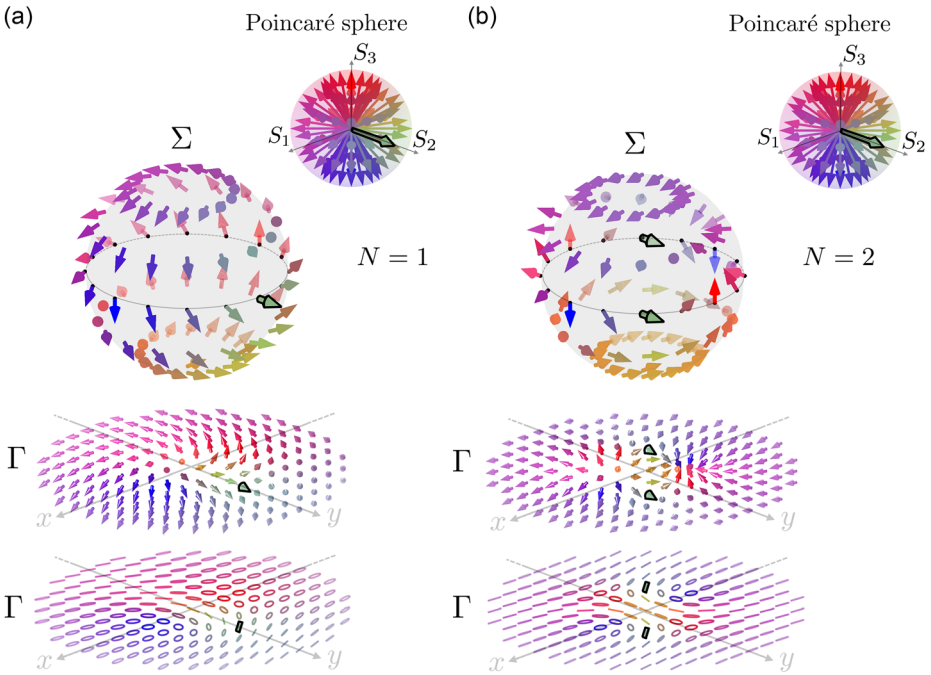

Figure 1. Paraxial optical fields (of bimerons) with skyrmion number a. $N = 1$ and b. $N = 2$. Reading from the bottom to the top, the polarization distribution on the plane Γ is represented in terms of polarization ellipses and above that as $\mathbf{S}(x, y)$ profile. The plane Γ was mapped onto a sphere Σ via an inverse stereographic projection, which in turn can be mapped onto the Poincaré sphere. For $N = 1$, Σ wraps once around the Poincaré sphere and for $N = 2$ twice. Consequently, the $\mathbf{S}_2$ vector, highlighted by a bold outline, appears once (twice) on Σ, and hence once (twice) in Γ for $N = 1$ ($N = 2$).

mappings shortly, once we have defined the skyrmion number. The skyrmion number N counts the number of times the tips of the vectors $\mathbf{S}(\mathbf{r})$ cover the entire Poincaré sphere. Figure 1a illustrates that for $N = 1$ the entire Poincaré sphere is covered once by $\mathbf{S}(\mathbf{r})$ and hence the $\mathbf{S}(x, y)$ distribution in the plane Γ contains all possible polarization states exactly once. Similarly, Figure 1b shows that for $N = 2$, the Poincaré sphere is covered twice by $\mathbf{S}(\mathbf{r})$, and all possible polarization states appear twice in Γ. Formally, the skyrmion number can be calculated from $\mathbf{S}(x, y)$ as

$$N = \frac{1}{4\pi}\int_{\Gamma} \mathbf{S} \cdot (\partial_x \mathbf{S} \times \partial_y \mathbf{S}) dx dy \tag{2}$$

Equation (2) measures the area on the Poincaré sphere covered by $\mathbf{S}$ as we explore the plane Γ as a fraction of the total area of the Poincaré sphere 4π.

In practice, the measured or simulated skyrmion number is often smaller than the true skyrmion number due to an incomplete mapping from Γ to Σ. For numerical simulations, this occurs due to the finite grid over which integration is performed. For experimental observations of skyrmions, errors occur due to numerical apertures that limit the accessible area within Γ, noise, especially at the beam periphery and in low-intensity regions, and insufficient measurement resolution that limits the capacity to capture variations of $\mathbf{S}(x, y)$.[11]

As paraxial optical skyrmions contain, by definition, all polarization states within their transverse profile they are, de facto, Poincaré beams.[31] The converse, however, is not true. First, the polarization state of Poincaré beams does not necessarily tend to the same value at spatial infinity. Second, skyrmions are constructed according to mapping rules, which do not have to apply for Poincaré beams.

3. Isolated Skyrmions

We shall now provide the rules for the mapping between Σ and the Poincaré sphere to construct the simplest type of optical paraxial skyrmions, which include Néel-type and Bloch-type skyrmions, anti-skyrmions, and bimerons.

We consider rational maps between two Riemann spheres as we wish to establish a correspondence between Σ and the Poincaré sphere. Stereographic projection relates a Skyrme field to a complex function with both zeros and poles. The zeros correspond to the South Pole of the sphere while the poles correspond to the North Pole. A rational map is a meromorphic function with this structure and a well-defined notion of degree. We interpret Γ as a complex plane and associate $(x, y) \in \Gamma$ with the stereographic coordinate $z = x + iy$ on Σ. This allows us to define a rational map of degree D as the function

$$R(z) = \frac{p(z)}{q(z)} \tag{3}$$

where p and q are polynomials of degree at most D with no common roots.[24] In analogy with Equation (1), the reduced Stokes vector $\mathbf{S}$ is then deduced from the rational map according to

$$\mathbf{S} = \frac{1}{1 + |R(z)|^2}(2\mathrm{Re}(R(z)), 2\mathrm{Im}(R(z)), -1 + |R(z)|^2) \tag{4}$$

We find that paraxial optical skyrmions of skyrmion number N can be built using rational maps of the form

$$R(z) = f(z)^{|N|} \tag{5}$$

This expression describes the simplest type of rational maps: polynomial functions with a single zero at $z = 0$. In two dimensions, the degree of a rational map is often called the winding number and measures how much the phase of a function changes as it "winds" round a zero. For the simplest complex function $f(z) = z = \mathbf{r}\exp(i\theta)$, Equation (5) becomes $R(z) = \mathbf{r}^{|N|}\exp(i|N|\theta)$ that changes by $2\pi|N|$ for a rotation around its zero, corresponding to Néel-type skyrmions with a winding number of $|N|$. The corresponding polarization texture $\mathbf{S}(x, y)$ is shown in **Figure 2**a. Similarly, anti-skyrmions, i.e., skyrmions of negative skyrmion number,[32] are generated by using the complex conjugate $f(z) = z^* = x - iy = \mathbf{r}\exp(-i\theta)$ (see Figure 2b). Complex conjugation effectively swaps the orientation of the skyrmion field. In the complex plane, this corresponds to a reflection of the real axis, whereas in the Poincaré sphere picture, it amounts to turning the sphere inside out. Bloch-type skyrmions, such as the one shown in Figure 2c, or any intermediate skyrmion for which the polarization state is right handed circularly polarized at infinity and left handed circularly polarized at the origin can be obtained by rotating the complex coordinate so that $f(z) = \exp(i\alpha)z$, with $\alpha = \pi/2$ corresponding to a Bloch-type skyrmion.

A uniform rotation of the local polarization vectors $\mathbf{S}$ generates different physical representations of the same polarization texture, featuring arbitrary orthogonal polarization states at infinity and at the center of the plane Γ. A $\pi/2$ rotation around the $\mathbf{S}_2$-axis, for example, will generate an in-plane skyrmion, also called a bimeron,[10,19] with orthogonal linearly polarized states at infinity and at the center as illustrated in Figure 2d. From a geometric point of view, a rotation of $\mathbf{S}$ simply induces a rotation of the Poincaré sphere, and hence does not change how many times $\mathbf{S}$ covers the Poincaré sphere.

The freedom to rotate $\mathbf{S}$ and $z = x + iy$ independently is a feature of the standard Skyrme model. In the context of the nuclear Skyrme model, these are referred to as *rotations* for the domain (here Σ) and *isorotations* for the target (here the Poincaré sphere).[33] Interestingly, the ability to perform these independent rotations is lost in magnetic skyrmions due the Dzyaloshinskii–Moriya interaction between neighboring magnetic spins, which leads to a modification of the total energy of the system, and which is invariant only under a combination of rotations and isorotations. This antisymmetric exchange interaction stems from a combined effect of spin–orbit coupling and broken inversion symmetry[34] and restrict the allowed skyrmion configurations. These constraints do not apply for optical skyrmions.

In condensed matter literature, exact skyrmion configurations constructed from rational maps have been used as starting points for numerical energy minimization to find stable configurations in realistic models.[35] The rational maps only give true energy minimizers in specific critically coupled models;[36] however, they still capture some features of realistic configurations,

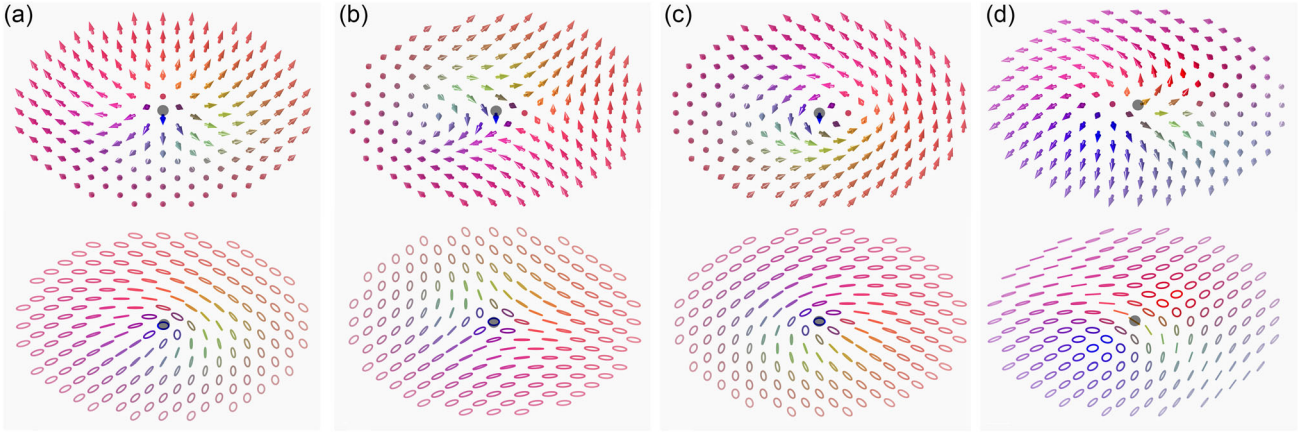

Figure 2. Polarization distribution depicted as a vector field $\mathbf{S}(x, y)$ (top row) and as distribution of polarization ellipses (bottom row) for a Néel-type skyrmion a), an anti-skyrmion b), a Bloch-type skyrmion c), and a bimeron d) based on Equation (3). Shaded disks indicate the position of the zeros of the associated rational map.

namely the skyrmion number. Similarly, rational maps provide excellent starting points for the physical realization of experimental paraxial optical skyrmion beams, as we shall now demonstrate.

To date, experimental paraxial skyrmion beams, $|\psi\rangle$, have mostly been generated by superposing a pair of orthogonally polarized Laguerre Gaussian (LG) modes[10,11]

$$|\psi\rangle = \frac{1}{\sqrt{2}}(\mathrm{LG}_{n_0}^{\ell_0}|0\rangle + \exp(i\phi)\mathrm{LG}_{n_1}^{\ell_1}|1\rangle) \tag{6}$$

where the bra-ket notation is used for convenience, $|0\rangle$ and $|1\rangle$ represent any two orthogonal polarization states, ϕ is an arbitrary phase factor, ℓ is the topological charge of the mode, counting the number of phase revolutions around the optical vortex, and n its radial order. We can, without loss of generality, ignore the phase factor $\exp(i\phi)$, as it does not affect the skyrmion number or indeed the intensity profile of $|\psi\rangle$. Equation (6) can then be rewritten in the compact form

$$|\psi\rangle = \frac{|0\rangle + \mu(\mathbf{r})|1\rangle}{\sqrt{1+|\mu(\mathbf{r})|^2}} \tag{7}$$

where $\mu(\mathbf{r}) = \mathrm{LG}_{n_1}^{\ell_1}/\mathrm{LG}_{n_0}^{\ell_0}$ is the ratio of the amplitude and phase product of the spatial modes, with an overall azimuthal phase proportional to $\ell_1 - \ell_0$. The spatial distribution $\mathbf{S}$ is obtained as follows

$$\mathbf{S}_i = \langle\psi|\sigma_i|\psi\rangle \tag{8}$$

where σ_i are the Pauli matrices, yielding

$$\mathbf{S} = \frac{1}{1+|\mu(\mathbf{r})|^2}(2\mathrm{Re}(\mu(\mathbf{r})), 2\mathrm{Im}(\mu(\mathbf{r})), 1-|\mu(\mathbf{r})|^2)^T \tag{9}$$

This is equivalent to Equation (4) as it corresponds to a stereographic projection via the South Pole, followed by a reflection to allow for comparison with our North Pole stereographic projection as introduced in Equation (1), and corresponding to the map

$$R(z) = \frac{1}{\mu^*(\mathbf{r})} \tag{10}$$

Note, however, that while rational maps are restricted to holomorphic functions, this is not the case in Equation (8), where μ can represent any complex function. **Figure 3** shows the phase and modulus distributions of $R(z)$ according to Equation (5) or (10) over a numerical grid of arbitrary size, up to an overall scaling factor. It can be further shown that Equation (4) and (9) yield similar $\mathbf{S}$ distributions, as illustrated in **Figure 4**, confirming that superposing LG modes naturally implements the rational map approach for the construction of optical skyrmion beams. Rational maps thus form a good starting point to designing paraxial skyrmions, where one should seek to match the zeros of the rational map with the zeros of a ratio of LG beams to obtain an experimentally feasible skyrmion configuration.

All optical skyrmions constructed using Equation (5) are isolated skyrmions: $R(z)$ presents one zero where $z = 0$. We have shown that Equation (5) introduces a unifying framework for Néel-type and Bloch-type skyrmions, antiskyrmions, and bimerons. Beam superposition methods to construct different types of optical single skyrmions have been outlined in ref. [10] The construction of optical multiskyrmions, a term borrowed from condensed matter research to refer to structures presenting several skyrmion zeros,[23] is not straightforward, unless one knows the rules for mapping Γ to Σ.

4. Multi-Skyrmions

Paraxial multi-skyrmion beams can be constructed by generalizing Equation (5). We start by noting that a map based on the function $f(z - z_j)$ will generate a skyrmion or anti-skyrmion centered at the position (x_j, y_j) in the plane Γ. Multiple skyrmions with individual skyrmion numbers M_j then arise from

$$R(z) = \prod_j (f(z - z_j))^{M_j} \tag{11}$$

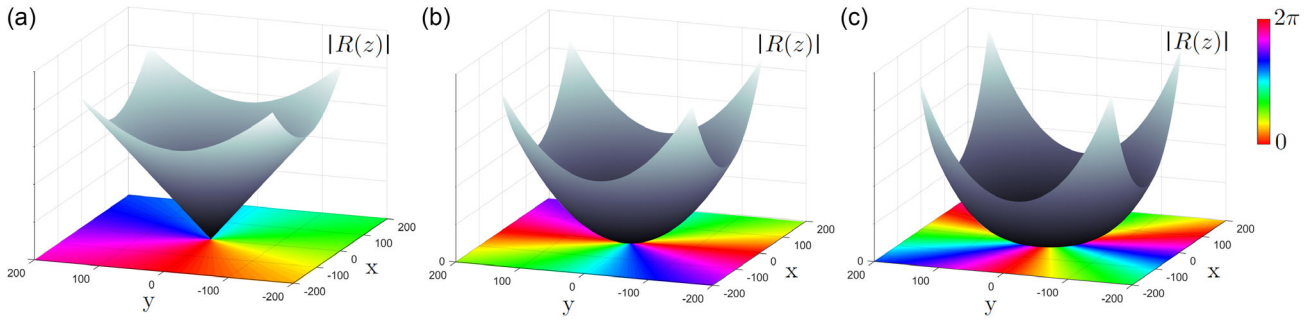

Figure 3. Phase profile (in hue colors) and associated modulus (gray surfaces in arbitrary units) of $R(z)$ for a skyrmion number of $N = 1, 2, 3$ a–c).

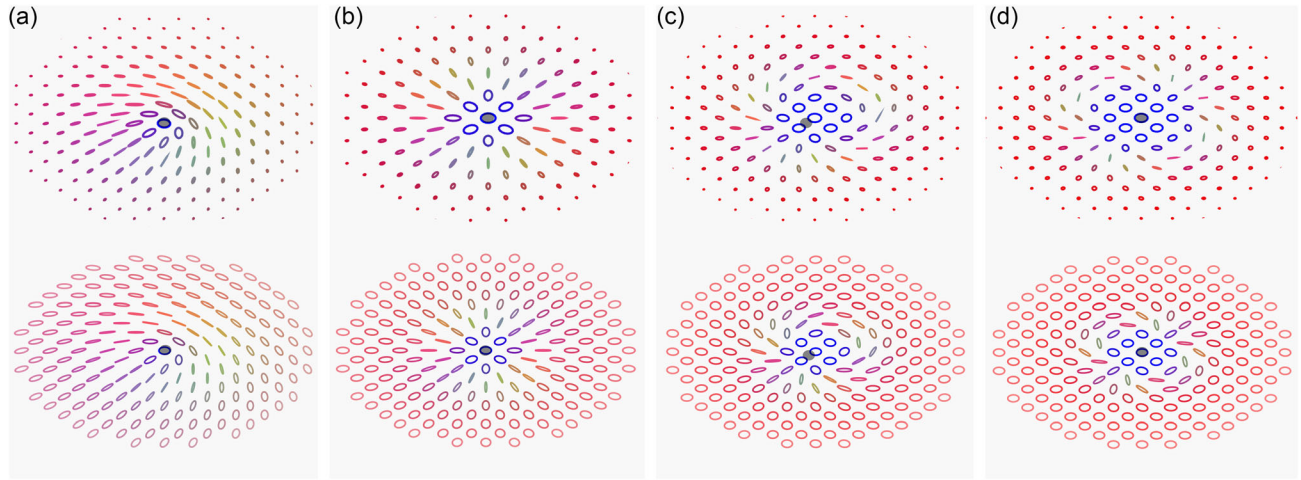

Figure 4. Polarization distributions of paraxial optical skyrmions of skyrmion number $N = 1$ to $N = 4$ in panels a–d), comparing experimentally accessible realizations in terms of superpositions of LG modes according to Equation (6) (upper row) and realizations according to the ideal rational map of Equation (5) (lower row). The former have finite beam waists, with varying intensity represented by the size of the ellipses. We have chosen the realization where $|0\rangle$ and $|1\rangle$ represent left- and right-handed polarization, respectively, and where $\ell_0 = 0$, $\ell_1 = 1$, $n_0 = n_1 = 0$. Shaded disks indicate the position of the skyrmion cores.

Figure 5 illustrates the polarization structures of various such multi-skyrmions. Panels a to c show: two $M = 1$ skyrmions at positions $(0, 1)$ and $(0, -1)$; the combination of a skyrmion and an anti-skyrmion centered at the same positions; two $M = 2$ skyrmions; and Figure 5d instead has four $M = 1$ skyrmions positioned at $(1, \pm 1)$ and $(-1, \pm 1)$. The polarization

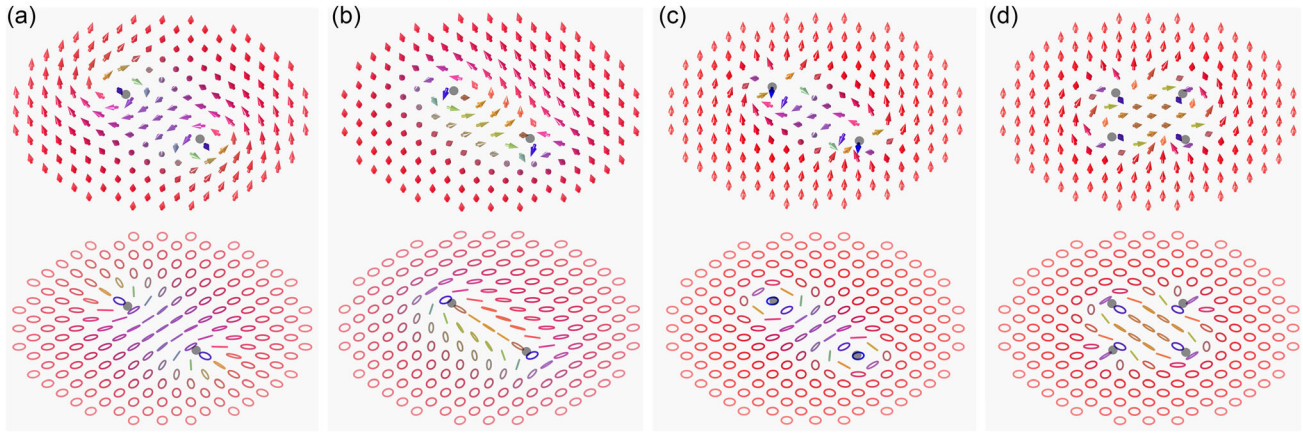

Figure 5. Polarization distributions represented as vector field and as distributions of polarization ellipses of two skyrmion zeros $M = 1$ a), one skyrmion zero and one antiskyrmion zero $M = 1$ b), two skyrmion zeros with $M = 2$ c), and four skyrmion zeros with $M = 1$ d). Shaded disks indicate the position of the skyrmion core.

distribution obtained in Figure 5a is similar to that of a magnetic bi-skyrmion such as the one presented in refs. [37,38] to describe two partially overlapping magnetic skyrmions.

By providing an analytical expression for multi-skyrmions, we have introduced guidelines for the experimental generation of multi-skyrmion fields. These may include, by extension of Equation (11), skyrmion lattices. We note, however, that the direct application of this Equation leads to issues in the simulated fields due to the overlap of the (potentially infinite) individual fields, which produces extremely narrow singularities or "melts" them together. Just like for magnetic skyrmions, rational maps may instead be taken as starting point for an optimization process based on energy or more generally stability constraints. If we follow the correspondence between rational maps and LG beams introduced in Equation (10), we can obtain guidelines for the experimental generation of optical multi-skyrmion beams. **Figure 6** shows the phase and modulus of the rational map defined in Equation (11) for two $M = 1$ skyrmions at positions $(0, 30)$ and $(0, -30)$. The phase profile clearly shows the two-phase singularities of unit winding number, indicating that this type of multi-skyrmion can be implemented experimentally by embedding optical vortices of unit topological charges at these locations, which is a simple task for state of the art light shaping techniques. From an experimental perspective, constructing multi-skyrmion beams can be seen as a phase engineering problem, involving the relative positioning of phase singularities.

By construction, each zero of the rational map contributes to the total skyrmion number by an amount given by the degree of the rational map, M_j. This suggests that we can split an optical skyrmion of skyrmion number N into several skyrmion zeros of total skyrmion number $N = \sum_j M_j$, or vice versa, combine multiple lower order skyrmions into a higher order one, although the latter process may not be entropically stable. Propagation studies such as[9] suggest that the skyrmion number is a conserved property in freely propagating isolated skyrmion beams. We anticipate that the total skyrmion number of a multi skyrmion beam will also be conserved upon free propagation, much like the topological charge of optical vortex beams. Skyrmion splitting

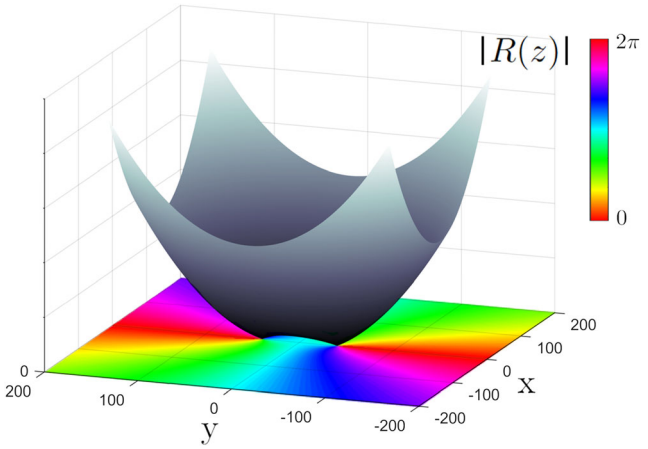

Figure 6. Phase profile (in hue colors) and associated modulus (gray surface) of $R(z)$ for a multi-skyrmion beam presenting two skyrmions ($M = 1$) at positions $(0, 30)$ and $(0, -30)$.

may be witnessed by perturbing vortex beams, in analogy to the effect in polarization[39,40] and phase vortices[41,42] dynamics. A specific case of vortex combination and splitting are linked to the annihilation and creation mechanisms of optical skyrmion zeros, including obtaining a skyrmion number of $N = 0$ by carefully combining skyrmion with anti-skyrmions. Mathematically, combining two individual skyrmions amounts to multiplying individual rational maps $f(z)^{|N|} \times f(z)^{|M|} = f(z)^{|N|+|M|}$, while combining a skyrmion with its respective antiskyrmion $z \times z^* = |z|^2$ yields nonhomogeneous polarization patterns of skyrmion number $N = 0$ as this process destroys the characteristic azimuthal polarization profile. Experimentally, increasing the skyrmion number entails merging individual phase vortices or increasing the topological charge of the individual LG mode to increase the difference $\ell_1 - \ell_0$ defining the phase profile of $\mu(\mathbf{r})$ in Equation (7). Identifying the correspondence between experimental procedures, including the action of q-plates, superpositions, and nonlinear processes, with a mathematical description in terms of rational maps will be a task for future studies.

5. Conclusion

We have shown that rational maps are the backbone of constructing paraxial optical skyrmion fields. Not only can they model single optical skyrmion fields, including Néel type and Bloch type skyrmions, antiskyrmions, and bimerons, but they can also be used to construct multi-skyrmions, paving the way for the controlled experimental realization of general optical skyrmion fields and enabling the study of skyrmion–skyrmion interactions in optical fields. The explicit rational maps, defined in Equation (5), correspond to the minimum energy configurations in the $O(3)$-sigma model.[30] Uncovering the equations that define paraxial optical skyrmions is of paramount importance as it constitutes the first step in understanding how optical skyrmion fields differ from their magnetic counterparts. We saw, for instance, that in contrast to magnetic skyrmions, the polarization and μ can be rotated independently, yielding different types of skyrmion configurations. This is not surprising as the freely propagating polarization textures are in principle only limited by Maxwell's equations. Optical skyrmion fields offer a versatile platform for the investigation of exotic topological structures, which are not otherwise supported in magnetism. In this article, we were concerned with optical skyrmions in a single plane, and the resulting structures are in general not eigenmodes of propagation. The rational map formalism introduced in this article lays the foundations for investigations confirming or ruling out the existence of stabilizing terms for optical skyrmion fields, which should be possible by studying their behavior upon perturbation or free propagation.

Acknowledgements

C.M.C. and S.F.-A. acknowledge financial support from the Royal Society through an International Newton fellowship NIF/R1/192384.

Conflict of Interest

The authors declare no conflict of interest.

Data Availability Statement

Data sharing is not applicable to this article as no new data were created or analyzed in this study.

Keywords

rational maps, skyrmion, structured light

Received: December 14, 2022
Revised: February 14, 2023
Published online: February 25, 2023

[1] T. Skyrme, *Nucl. Phys.* **1962**, *31*, 556.
[2] N. S. Manton, *Commun. Math. Phys.* **1987**, *111*, 469.
[3] J. Han, *Modern Physics*, Springer International Publishing, Cham, Switzerland **2017**, https://doi.org/10.1007/978-3-3.
[4] T. Sakai, S. Sugimoto, *Prog. Theor. Phys.* **2005**, *113*, 843.
[5] A. N. Bogdanov, C. Panagopoulos, *Nat. Rev. Phys.* **2020**, *2*, 492.
[6] R. D. Muelas-Hurtado, K. Volke-Sepúlveda, J. L. Ealo, F. Nori, M. A. Alonso, K. Y. Bliokh, E. Brasselet, *Phys. Rev. Lett.* **2022**, *129*, 204301.
[7] S. Tsesses, E. Ostrovsky, K. Cohen, B. Gjonaj, N. H. Lindner, G. Bartal, *Science* **2018**, *361*, 993.
[8] L. Du, A. Yang, A. Zayats, *Nat. Phys.* **2019**, *15*, 650.
[9] S. Gao, F. C. Speirits, F. Castellucci, S. Franke-Arnold, S. M. Barnett, J. B. Götte, *Phys. Rev. A* **2020**, *102*, 053513.
[10] Y. Shen, E. C. Martnez, C. Rosales-Guzmán, *ACS Photonics* **2022**, *1*, 296.
[11] A. McWilliam, C. M. Cisowski, Z. Ye, F. C. Speirits, J. B. Götte, S. M. Barnett, S. Franke-Arnold, https://arxiv.org/abs/2209.06734 (accessed: September 2022).
[12] R. Gutiérrez-Cuevas, E. Pisanty, *J. Opt.* **2021**, *23*, 024004.
[13] P. Ornelas, I. Nape, R. d. M. Koch, A. Forbes, https://arxiv.org/abs/2210.04690 (accessed: September 2022).
[14] D. Sugic, R. Droop, E. Otte, D. Ehrmanntraut, F. Nori, J. Ruostekoski, C. Denz, M. R. Dennis, *Nat. Commun.* **2021**, *12*, 6785.
[15] Y. Shen, B. Yu, H. Wu, C. Li, Z. Zhu, A. V. Zayats, *Adv. Photonics* **2023**, *5*, 015001.
[16] Y. Shen, Q. Zhang, P. Shi, L. Du, A. V. Zayats, X. Yuan, https://arxiv.org/abs/2205.10329 (accessed: June 2022).
[17] B. Piette, H. Müller-Kirsten, D. Tchrakian, W. Zakrzewski, *Phys. Lett. B* **1994**, *320*, 294.
[18] B. M. A. G. Piette, B. J. Schroers, W. J. Zakrzewski, *Z. Phys. C Part. Fields* **1995**, *65*, 165.
[19] Y. Shen, *Opt. Lett.* **2021**, *46*, 3737.
[20] C. D. Stanciu, F. Hansteen, A. V. Kimel, A. Kirilyuk, A. Tsukamoto, A. Itoh, T. Rasing, *Phys. Rev. Lett.* **2007**, *99*, 047601.
[21] C.-H. Lambert, S. Mangin, B. S. D. C. S. Varaprasad, Y. K. Takahashi, M. Hehn, M. Cinchetti, G. Malinowski, K. Hono, Y. Fainman, M. Aeschlimann, E. E. Fullerton, *Science* **2014**, *345*, 1337.
[22] A. Fert, V. Cros, J. Sampaio, *Nat. Nanotechnol.* **2013**, *8*, 152.
[23] D. Foster, C. Kind, P. J. Ackerman, J.-S. B. Tai, M. R. Dennis, I. I. Smalyukh, *Nat. Phys.* **2019**, *15*, 655.
[24] C. J. Houghton, N. S. Manton, P. M. Sutcliffe, *Nucl. Phys. B* **1998**, *510*, 507.
[25] R. A. Barrye, P. M. Sutcliffe, *Rev. Math. Phys.* **2002**, *14*, 29.
[26] S. K. Donaldson, *Commun. Math. Phys.* **1984**, *96*, 387.
[27] A. M. Polyakov, A. A. Belavin, *JETP Lett.* **1975**, *22*, 245.
[28] I. Hen, M. Karliner, *Phys. Rev. E* **2008**, *77*, 036612.
[29] N. Nagaosa, Y. Tokura, *Nat. Nanotechnol.* **2013**, *8*, 899.
[30] N. Manton, P. Sutcliffe, *Mathematical Physics*, Cambridge University Press, Cambridge, United Kingdom **2004**.
[31] A. M. Beckley, T. G. Brown, M. A. Alonso, *Opt. Express* **2010**, *18*, 10777.
[32] A. A. Kovalev, S. Sandhoefner, *Front. Phys.* **2018**, *6*, 98.
[33] N. S. Manton, *Skyrmions – A Theory of Nuclei*, World Scientific Publishing Europe Ltd., London, United Kingdom **2022**.
[34] D. Treves, S. Alexander, *J. Appl. Phys.* **1962**, *33*, 1133.
[35] V. M. Kuchkin, B. Barton-Singer, F. N. Rybakov, S. Blügel, B. J. Schroers, N. S. Kiselev, *Phys. Rev. B* **2020**, *102*, 144422.
[36] B. Barton-Singer, C. Ross, B. J. Schroers, *Commun. Math. Phys.* **2020**, *375*, 2259.
[37] X. Z. Yu, Y. Tokunaga, Y. Kaneko, W. Z. Zhang, K. Kimoto, Y. Matsui, Y. Taguchi, Y. Tokura, *Nat. Commun.* **2014**, *5*, 3198.
[38] B. Göbel, J. Henk, I. Mertig, *Sci. Rep.* **2019**, *9*, 9521.
[39] E. Otte, C. Alpmann, C. Denz, *Laser Photonics Rev.* **2018**, *12*, 1700200.
[40] A. D'Errico, M. Maffei, B. Piccirillo, C. de Lisio, F. Cardano, L. Marrucci, *Sci. Rep.* **2017**, *7*, 40195.
[41] F. Ricci, W. Löffler, M. van Exter, *Opt. Express* **2012**, *20*, 22961.
[42] A. A. Voitiv, J. M. Andersen, P. C. Ford, M. T. Lusk, M. E. Siemens, *Opt. Lett.* **2022**, *47*, 1391.